Mitigating disorder-induced zero-energy states in weakly coupled superconductor-semiconductor hybrid systems

Oladunjoye A. Awoga [1,*] Martin Leijnse,[1] Annica M. Black-Schaffer [2] and Jorge Cayao [2,†]
[1]*Solid State Physics and NanoLund, Lund University, Box 118, 22100 Lund, Sweden*
[2]*Department of Physics and Astronomy, Uppsala University, Box 516, 751 20 Uppsala, Sweden*

(Received 16 December 2022; revised 15 May 2023; accepted 16 May 2023; published 30 May 2023)

Disorder has appeared as one of the main mechanisms to induce topologically trivial zero-energy states in superconductor-semiconductor systems, thereby challenging the detection of topological superconductivity and Majorana bound states. Here, we demonstrate that, for disorder in any part of the system, the formation of disorder-induced trivial zero-energy states can, to a large extent, be mitigated by keeping the coupling between the semiconductor and superconductor weak. The only exception is strong disorder in the semiconductor, where instead the strong-coupling regime is somewhat more robust against disorder. Furthermore, we find that the topological phase in this weak-coupling regime is robust against disorder, with a large and well-defined topological gap which is highly beneficial for topological protection. Our work shows the advantages and disadvantages of weak and strong couplings under disorder, important for designing superconductor-semiconductor hybrid structures.

DOI: 10.1103/PhysRevB.107.184519

I. INTRODUCTION

Superconductor-semiconductor (SC-SM) hybrid systems have received much attention in the last 10 years due to their potential for the realization of topological superconductivity and Majorana bound states (MBSs) [1–9]. MBSs have been predicted to appear under a strong applied magnetic field, emerging at zero energy and located at the ends of the system [10–12]. Although multiple detection schemes of MBSs have been reported, quantized zero-bias conductance peaks have been one of the most pursued signatures [13–16], motivating many transport-based experiments to detect MBSs [17–24]. However, it is clear by now that zero-bias peaks do not necessarily represent evidence of MBSs because topologically trivial zero-energy states (TZESs) can also produce similar signatures [7,25–41].

Among the most relevant mechanisms known to cause the formation of TZESs are spatial inhomogeneities in the effective chemical potential profile of the SM [7,31,36,42,43]. Such spatial variations can occur due to distinct effects, such as gate voltages [44], finite-size effects of the SC [45–48], and random fluctuations due to charge inhomogeneities or generally scalar disorder [49–59]. While the effect of gates can, in principle, be controlled [44,60], the size of the SC and disorder are much harder to avoid in real samples. In fact, recent measurements of zero-bias peaks have been interpreted in terms of disorder-induced TZESs [22,61–63], suggesting disorder is the main obstacle to realize MBSs [64–66]. Also, it has been shown that the coupling between the SC and SM considerably affects the low-energy properties. In particular, strong couplings, seen earlier as favorable due to the large induced gaps in the SM [67], induce detrimental effects such as renormalization of the physical parameters of the SM, the need of large Zeeman fields to reach the topological phase, and also the formation of TZESs [45–47,68]. As a result, the interplay of disorder and SC-SM coupling challenges the realization of topological superconductivity.

In this work we study the influence of scalar disorder in SC-SM hybrid systems and show that its impact can largely be suppressed in the weak SC-SM coupling regime. In particular, we discover that disorder in any part of the system does not induce TZESs, in stark contrast to the strong-coupling regime. We find that this effect holds for a broad range of disorder strengths when present in the SM, SC, or the coupling. We find the only exception to be the case of very strong disorder in the SM; there, the strong-coupling regime shows better resilience against disorder. We also obtain that the topological phase in the weak-coupling regime is robust against strong disorder, with a well-defined topological gap and the absence of disorder-induced in-gap states. Our results thus allow tailoring the coupling strength depending on the dominant sources of disorder, which is relevant when designing efficient superconductor-semiconductor systems.

II. SC-SM MODEL

We consider a disordered SC-SM system formed by coupling a two-dimensional (2D) conventional spin-singlet

*oladunjoye.awoga@ftf.lth.se
†jorge.cayao@physics.uu.se

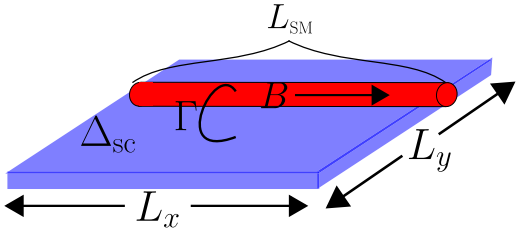

FIG. 1. Schematics of the system: SM (red) of length $L_{\rm SM}$ in a parallel magnetic field B coupled through Γ to a thin-film conventional SC of length L_x and width L_y (blue). Part of the SM is not coupled to the SC, thus remaining in the normal state, giving rise to a SCN junction.

s-wave SC and a one-dimensional (1D) SM nanowire with strong spin-orbit coupling under a Zeeman field B, as shown in Fig. 1. This coupled model goes beyond the usual 1D effective description and captures several realistic properties of SC-SM systems [45–47,69–71], such as the renormalization of all parameters in the SM and not just the inclusion of superconductivity, the hybridization between the SM and SC, and the quality of the SC-SM interface (see also Refs. [1–8]). Disorder is taken into account in the form of nonmagnetic scalar disorder [72], as it is likely the most unavoidable type of disorder present in all the regions of the SC-SM system [22,61–66,73,74]. For instance, charge puddles or inhomogeneities lead to scalar disorder in the chemical potential of the SM and SC, and despite advances in device fabrication, the interface between the SC and SM still suffers from imperfections, leading to disorder in the coupling (or hybridization) strength Γ between the SC and SM. We thus model the total SC-SM system by $H = H^{\rm c} + H^{\rm d}$, where $H^{\rm c(d)} = H^{\rm c(d)}_{\rm SM} + H^{\rm c(d)}_{\rm SC} + H^{\rm c(d)}_{\Gamma}$. Here, $H^{\rm c}$ describes the clean (c) system, while $H^{\rm d}$ models the disorder (d). The clean system is given by

$$\begin{aligned} H^{\rm c}_{\rm SM} &= \sum_{r,r'\beta,\beta'} d^\dagger_{r\beta}\big[\big(\varepsilon_{\rm SM} + B\sigma^x_{\beta\beta'}\big)\delta_{rr'} \\ &\quad - \big(t_{\rm SM} - i\alpha_{\rm SM}\sigma^y_{\beta\beta'}\big)\delta_{\langle r,r'\rangle}\big]d_{r'\beta'} + \text{H.c.}, \\ H^{\rm c}_{\rm SC} &= \sum_{j,j',\beta} c^\dagger_{j\beta}\big[\varepsilon_{\rm SC}\delta_{jj'} - t_{\rm SC}\delta_{\langle j,j'\rangle}\big]c_{j'\beta} \\ &\quad + \sum_{j,\beta,\beta'} c^\dagger_{j\beta}\big[i\Delta_{\rm SC}\sigma^y_{\beta\beta'}\big]c^\dagger_{j\beta'} + \text{H.c.}, \\ H^{\rm c}_{\Gamma} &= -\sum_{r,j,\beta} c^\dagger_{j\beta}\big[\Gamma\delta_{j_x,r}\delta_{j_y,\frac{L_y+1}{2}}\big]d_{r\beta} + \text{H.c}, \end{aligned} \tag{1}$$

where $d_{r,\beta}$ destroys an electron with spin β at site r in the 1D SM of length $L_{\rm SM}$, $c_{m,\beta}$ destroys an electron with spin β at site $j = (j_x, j_y)$ in the 2D SC, $\delta_{\langle\cdots\rangle}(\delta_{jj'})$ enforces only nearest-neighbor (on-site) terms, and σ^n is the n-Pauli matrix in spin space. Also, $\varepsilon_{\rm SM} = (2t_{\rm SM} - \mu_{\rm SM})$ is the SM on-site energy, $\varepsilon_{\rm SC} = (4t_{\rm SC} - \mu_{\rm SC})$ is the SC on-site energy, $\mu_{\rm SM(SC)}$ is the SM (SC) chemical potential, $t_{\rm SM(SC)}$ is the nearest-neighbor hopping in the SM (SC), $\alpha_{\rm SM}$ is the Rashba spin-orbit coupling in the SM, $\Delta_{\rm SC}$ is the on-site s-wave order parameter associated with conventional superconductivity, and B is the external Zeeman field. To model scalar disorder, we consider random site-dependent fluctuations in the chemical potential of the SM and SC, as well as random fluctuations in the coupling strength Γ, given by

$$\begin{aligned} H^{\rm d}_{\rm SM} &= \sum_{r\beta} d^\dagger_{r\beta}[\delta\mu_{\rm SM}(r)]d_{r\beta} + \text{H.c.}, \\ H^{\rm d}_{\rm SC} &= \sum_{j\beta} c^\dagger_{j\beta}[\delta\mu_{\rm SC}(j)]c_{j\beta} + \text{H.c.}, \\ H^{\rm d}_{\Gamma} &= -\sum_{r,j\beta} c^\dagger_{j\beta}\big[\delta\Gamma(j)\delta_{j_x,r}\delta_{j_y,\frac{L_y+1}{2}}\big]d_{r\beta} + \text{H.c.}, \end{aligned} \tag{2}$$

where $\delta Q(n) \in [-w_Q, w_Q]$ describes the site-dependent random fluctuations in the quantity $Q = \{\mu_{\rm SC}, \mu_{\rm SM}, \Gamma\}$, with w_Q being the disorder strength. This approach ensures that $\langle\delta Q\rangle = 0$. To characterize the relative strength of the disorder, we generally compare the strength with respect to the quantity in the clean regime, w_Q/Q.

In terms of parameters, we consider realistic values often used to describe SC-SM systems [45–47,58]. In particular, for the SC we use $|\Delta_{\rm SC}| = 0.1t_{\rm SC}$, $\mu_{\rm SC} = 0.38t_{\rm SC}$, and $L_y = 11a$, with a being the discretization parameter. In the SM, we set $L_{\rm SM} = 1000a$, $\mu_{\rm SM} = 0.02t_{\rm SM}$, $\alpha_{\rm SM} = 0.05t_{\rm SM}$, and $t_{\rm SM} = 4t_{\rm SC}$, which incorporates the mismatch in the lattice constants and effective masses of the SM and SC. We further leave a small part of the SM uncovered by the SC in order to model a superconductor-normal (SCN) junction, often used in transport experiments [7]. To eliminate the presence of low-energy states and avoid severe gating effects in N, we keep N very short with $L_{\rm N} = 2a$ [75]. The physics of SC-SM systems also heavily depends on the coupling Γ [45]. In fact, the induced gap exhibits a linear dependence on the coupling strength at weak Γ, while it has a nonlinear behavior at stronger Γ, which eventually saturates at the values of the parent superconductor gap $\Delta_{\rm SC}$. This behavior of the induced gap enables us to identify two distinct regimes, which we refer to as the *weak-coupling regime*, with an induced gap linear in Γ, and the *strong-coupling regime*, with an induced gap nonlinear with Γ. There is no sharp boundary between the weak- and strong-coupling regimes, but there is a smooth crossover that needs to be avoided when targeting either regime. For the above parameters, we have identified that the border between weak and strong coupling occurs for $\Gamma/t_{\rm SC} \sim 0.4$ [45]. Therefore, we choose $\Gamma/t_{\rm SC} = 0.3$ and $\Gamma/t_{\rm SC} = 0.7$ as representative values of the weak- and strong-coupling regimes, respectively. We also note that, since the induced gap reaches $\Delta_{\rm SC}$ at $\Gamma/t_{\rm SC} = 1$, there is no reason to consider $\Gamma/t_{\rm SC} > 1$ for the strong-coupling regime. Finally, for the considered parameters, we estimate that the disorder can be considered to be strong for $w_{\mu_{\rm SC}}/\mu_{\rm SC} \gtrsim 0.8$, $w_{\mu_{\rm SM}}/\mu_{\rm SM} \gtrsim 1$, and $w_\Gamma/\Gamma \gtrsim 0.3$; see Appendix A for details. Since we are interested in the role of disorder for inducing TZESs, we numerically solve the full SC-SM Hamiltonian H and focus on the low-energy spectrum. We employ the Arnoldi iteration method [76] because it efficiently allows us to address large systems.

A. Clean regime

Without disorder, the region of the SM that is in contact with the SC undergoes a topological phase transition (TPT) at a critical field $B_{\rm c}$ and enters into a topological phase where

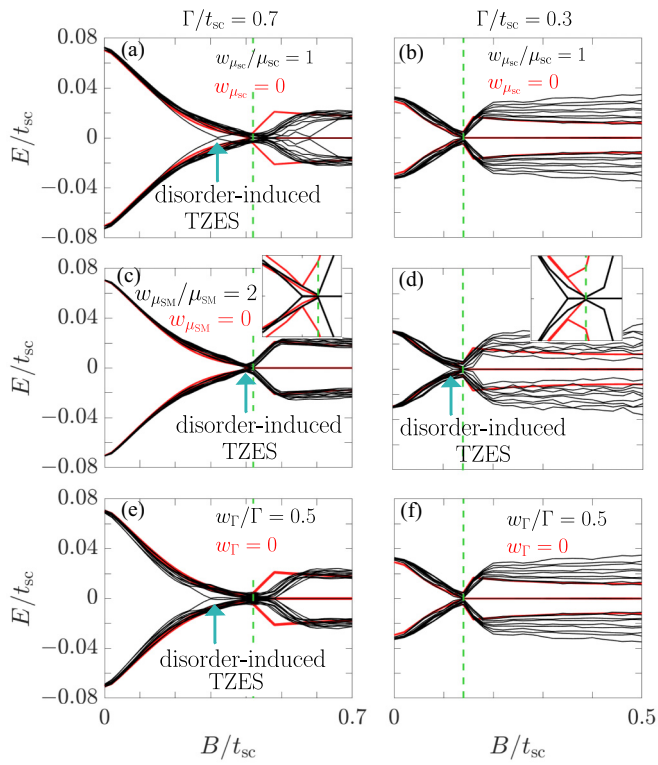

FIG. 2. Low-energy spectrum as a function of the Zeeman field B for a single realization (20 lowest levels, black) for disorder in (a) and (b) the SC and (c) and (d) SM and (e) and (f) at the interface for strong (left) and weak (right) coupling Γ. The chosen values of disorder correspond to strong disorder (see text). Insets show zooms around the TPT (dashed green line). Clean system spectrum (four lowest levels, red).

MBSs emerge at the end points of the SM [10–12,77]. Under ideal conditions, the topological properties can be understood from the two lowest energy levels, $E_{0,1}$. In the trivial phase at $B = 0$, the induced gap is defined by E_0, which decreases as B increases until it reaches zero at the TPT [78]. After the TPT, the induced gap reopens, but now it is defined by E_1, while E_0 sticks to zero energy for long enough SMs, revealing the MBSs. The induced gap in the topological phase (the topological gap) isolates the MBSs from the quasi-continuum and thus provides protection [79].

III. DISORDER-INDUCED TZESs

We next analyze the SC-SM system under disorder in the SC and SM and at the SC-SM interface, as described by Eq. (2), and separate the behavior for weak and strong coupling Γ. In Fig. 2 we show the low-energy spectrum as a function of B under a single, but representative [80], realization of strong disorder (black) in the SC [Figs. 2(a) and 2(b)] and SM [Figs. 2(c) and 2(d)] and at the interface [Figs. 2(e) and 2(f)] for strong (left) and weak (right) coupling. To contrast the disordered results, we also show the four lowest energy levels of the clean system (red), which display a clear TPT (dashed green line) and no TZESs.

For strongly coupled SC-SM systems ($\Gamma/t_{\rm SC} = 0.7$), the immediate observation is that finite disorder in the SC or at the interface induces TZESs well before the TPT [Figs. 2(a) and 2(e)]. The high impact of disorder in this regime occurs due to the large renormalization induced by the SC on the SM parameters. Specifically, the chemical potential of the SM acquires a highly inhomogeneous spatial profile that can confine zero-energy states [45]. Disorder in the SM seems to be less detrimental, as it affects only the trivial phase just before the TPT, but also technically induces TZESs [Fig. 2(c)]. We find that these TZESs are largely spatially located throughout the SC and also remain if we remove the SCN junction [81]. We note here that the presence of TZESs does not violate Anderson's theorem about disorder robustness in s-wave superconductors [82] since they occur in a regime where time-reversal symmetry is broken and effective p-wave spin-triplet superconducting correlations form [83–91]. Furthermore, we note that for disorder in the SC or at the interface [Figs. 2(a) and 2(e)], it is hard to discern the TPT and gap closing in the strong-coupling regime due to an accumulation of low-energy states on both sides of the TPT [58,59,62,63]. This reduces the topological gap and even leads to the appearance of low-energy levels that coexist with MBSs above the TPT. Therefore, disorder in the SC and at the interface is highly detrimental for MBSs in the strong-coupling regime.

For weakly coupled SC-SM systems ($\Gamma/t_{\rm SC} = 0.3$) we find that the impact of disorder on the low-energy spectrum is surprisingly largely absent, provided the strengths of disorder do not considerably surpass the values of their respective quantities in the clean regime [Figs. 2(b), 2(d) and 2(f)]. In particular, the low-energy spectrum exhibits a behavior similar to that in the clean regime with no induced TZESs, thus revealing an important advantage over the strong-coupling regime [58,59,62,63]. While this behavior practically occurs for disorder in all regions, it is fair to notice that the strong coupling reflects more resilience for disorder in the SM [Figs. 2(c) and 2(d)]. As no disorder-induced TZESs appear in the weak-coupling regime, the TPT is also easily identified by the naked eye, unlike in the strong-coupling regime. Furthermore, in the topological phase above the TPT, the low-energy spectrum reveals the emergence of MBSs and a finite topological gap, both highly robust against disorder for weak coupling. We note that the stability of the topological gap against disorder in the SC for weak Γ is in line with Ref. [54], which showed that the impurity scattering rate in the SC involves higher-order tunneling processes and is suppressed due to the destructive quantum interference of quasiparticle and quasihole trajectories. In a broader perspective, the robustness against disorder in both the trivial and topological phases in the weak-coupling regime originates from the vanishing renormalization of the effective chemical potential in the SM for weak Γ [92]. To further explore the impact of disorder, we verify that the weak-coupling regime remains robust in a realistic scenario with disorder in all parts of the system (see Appendix B). These results clearly demonstrate the advantages and disadvantages of weak and strong couplings in disordered SC-SM systems.

In order to obtain further understanding of the role of disorder, we show in Figs. 3(a)–3(c) the number of disorder configurations that produce disorder-induced TZESs N, obtained by analyzing 30 random disorder realizations, as a function of disorder strength for all three types of disorder

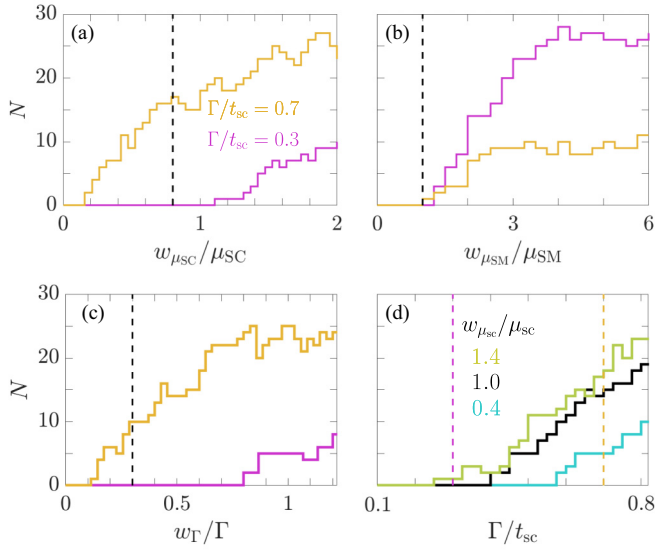

FIG. 3. Number of disorder configurations N resulting in disorder-induced TZES (out of 30 random realizations) as a function of disorder strength at weak (yellow) and strong (purple) coupling Γ for disorder in (a) the SC and (b) SM and (c) at the interface. Vertical black dashed lines indicate the boundary between weak (left side) and strong (right side) disorder. (d) N as a function of coupling strength for disorder in the SC at different disorder strengths. Vertical colored lines denote $\Gamma/t_{SC} = 0.3, 0.7$.

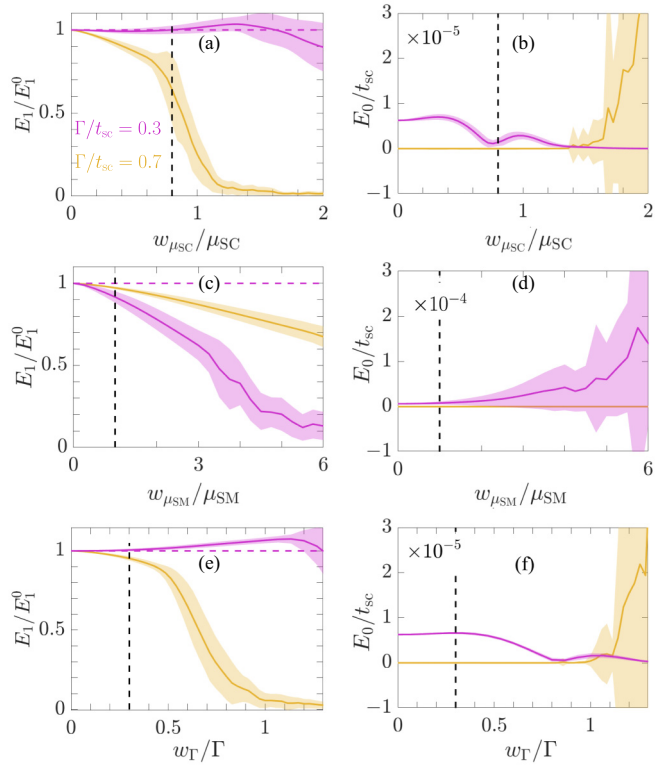

FIG. 4. Disorder-averaged calculations (30 random configurations) in the topological phase at $B/B_c = 1.5$ showing E_1/E_1^0 (left) and E_0/t_{SC} (right) as a function of disorder strength for disorder in (a) and (b) the SC and (c) and (d) SM and (e) and (f) at the interface for weak (purple) and strong (yellow) coupling Γ. Shaded regions represent one standard deviation. Vertical black dashed lines indicate the boundary between weak (left) and strong (right) disorder.

considered. We here count only disorder configurations that induce clearly isolated TZESs, like those seen in Fig. 2, in the Zeeman field range $B \in [0, B_c]$. As the disorder strength increases, N also increases but with a very different behavior for weak (purple) and strong (yellow) coupling Γ. Notably, for disorder both in the SC and at the interface, disorder-induced TZESs already form for very weak disorder at strong coupling Γ, while very strong disorder is required for TZESs to appear in the weak-coupling regime [Figs. 3(a) and 3(c)]. In fact, in the latter situation, the disorder is often strong enough to also destroy superconductivity within a self-consistent calculation [93]. On the other hand, for disorder in the SM, disorder-induced TZESs form for only very strong disorder in both the weak- and strong-coupling regimes [Fig. 3(b)]. Thus, while it is always possible to avoid disorder-induced TZESs in weakly coupled SC-SM systems, disorder-induced TZESs can be avoided in strongly coupled SC-SM systems only for disorder in the SM. To further inspect the robustness of the weak-coupling regime, in Fig. 3(d) we plot N as a function of Γ for different strengths of disorder in the SC. The overall observation is that there always exists a regime at weak Γ where no disorder-induced TZESs appear, with weaker coupling requiring ever stronger disorder to form TZESs. We find similar results for disorder in the SM and at the interface. Thus, we find that it is possible to avoid disorder-induced TZESs in SC-SM systems even beyond the strong-disorder limit as long the SC-SM coupling is kept weak.

IV. ROBUSTNESS OF TOPOLOGICAL PHASE

Finally, we explore the role of disorder in the topological phase, focusing on the two lowest levels, $E_{0,1}$, because they determine the presence of MBSs (topological gap). In Fig. 4 we plot the disorder-averaged E_0 (left) and E_1 (right) at fixed B/B_c beyond the TPT as a function of the disorder strength for disorder in the SC (top), in the SM (middle), and at the interface (bottom) for both the weak (purple) and strong (yellow) coupling regimes. The calculations correspond to 30 random disorder configurations with the standard deviation indicated (shaded regions), but we find that the results remain unchanged for an increased number of configurations. By direct inspection we note that E_0 and E_1 strongly depend on the strength of disorder, with nontrivial behavior for weak and strong Γ. First, focusing on the topological gap E_1, we find that as disorder in the SC or at the interface increases, E_1 undergoes a notably fast reduction in the strong-coupling regime, acquiring a vanishing value just beyond what we characterize as the strong-disorder regime [Figs. 4(a) and 4(e)]. In contrast, E_1 remains robust for weak coupling and becomes even larger than the clean reference value E_1^0 (dashed line) for large and even strong disorder; it decreases only for very strong disorder, at first with increased spread [purple in Figs. 4(a) and 4(e)]. While the robustness of the topological phase under weak disorder was reported earlier [93,94], we emphasize that the robustness of the weak-coupling regime seen here occurs even under strong disorder strengths for disorder either in the SC or at the interface. For disorder in

the SM, however, we find a faster reduction of the topological gap in the weak-coupling regime than for strong coupling, but the reduction is significant only for very strong disorder, such that the gap is largely preserved in both coupling regimes for weak to strong disorder.

For the lowest energy level E_0, representing the MBSs, we find a similar disorder robustness for disorder both in the SC and at the interface for weak coupling [purple in Figs. 4(b) and 4(f)]. In particular, while weak SC-SM coupling results in the E_0 level not being at zero energy in the clean system due to a finite Majorana localization length, disorder actually pushes this E_0 level towards zero by promoting smaller localization lengths, consistent with the increased topological gap. Thus, the MBSs become more localized for finite disorder in the SC and at the interface in the weak-coupling regime. In contrast, for strong coupling, E_0 clearly starts at zero energy in the clean regime but then with increasing disorder becomes finite and also heavily dependent on the specific disorder configuration, as seen by the large spread. The behavior is again different for disorder in the SM, where E_0 instead increases more with disorder at weak coupling than at strong coupling, but, again, the effect is not very noticeable until very strong disorder is considered. Taken together, the reduction in E_0 and small increase in E_1 with increasing disorder strength for disorder both in the SC and at the interface, together with an overall stability against disorder in the SM, imply that the topological phase in weakly coupled SC-SM systems is very robust in the full range of weak to moderately strong disorder. In contrast, strongly coupled SC-SM systems show a pronounced fragility towards disorder both in the SC and at the interface, which stems from the strong renormalization caused in the SM parameters. In all of the above results we consider systems in which there are no TZESs in the clean regime, but we have verified that the results remain even if the clean system already hosts TZESs, e.g., due to an interplay of the finite size of the SC and strong coupling (see Appendix C).

V. CONCLUSIONS

To summarize, the weak-coupling regime in SC-SM systems is robust against weak to moderately strong disorder and offers a powerful way to mitigate the formation of disorder-induced TZESs, in contrast to what has been reported for strong coupling [58,59,62,63]. Furthermore, disorder in the SC or at the interface can even help generate more stable MBSs and a larger topological gap, both beneficial properties for designing future SC-SM structures with enhanced topological protection. At the same time, strongly coupled systems are more stable against very strong disorder in the SM. After having identified how to mitigate the detrimental impact of disorder in SC-SM systems, the next step towards modeling realistic Majorana devices may include electrostatic effects [95–99] and multichannel SMs [100–104]. Our work thus illustrates the advantages and disadvantages of weakly and strongly coupled SC-SM systems under scalar disorder of potential use for simulating and understanding actual Majorana experiments.

ACKNOWLEDGMENTS

O.A.A. and M.L. acknowledge funding from NanoLund, the Swedish Research Council (VR), and the European Research Council (ERC) under the European Union's Horizon 2020 research and innovation programme under Grant Agreement No. 856526. J.C. acknowledges financial support from the Swedish Research Council (Vetenskapsrådet Grant No. 2021-04121), the Göran Gustafsson Foundation (Grant No. 2216), and the Carl Trygger Foundation (Grant No. 22: 2093). A.M.B.-S. acknowledges financial support from the Swedish Research Council (Vetenskapsrådet Grant No. 2018-03488) and the Knut and Alice Wallenberg Foundation through the Wallenberg Academy Fellows program. Simulations were enabled by resources provided by the Swedish National Infrastructure for Computing (SNIC) at the High Performance Computing Center North (HPC2N), Kebnekaise cluster, partially funded by the Swedish Research Council through Grant No. 2018-05973.

APPENDIX A: ESTIMATION OF DISORDER STRENGTH

In the main text we stated that disorder is strong when $w_{\mu_{\rm SC}}/\mu_{\rm SC} \gtrsim 0.8$, $w_{\mu_{\rm SM}}/\mu_{\rm SM} \gtrsim 1$, and $w_\Gamma/\Gamma \gtrsim 0.3$ for disorder in the SC and SM and at the interface, respectively. In this Appendix, we provide the details of this estimation.

We characterize the regimes of disorder in the SC and SM using the ratio ξ/l, where l the mean free path and ξ is the superconducting coherence length [105]. When the ratio ξ/l is used, it is standard to classify the regime with $\xi/l \ll 1$ as a weak disordered regime, while $\xi/l \gtrsim 1$ denotes strong disorder. Here, the mean free path is given by $l = v_{\rm F}/\pi N(0) w^2_{\rm SC,SM}$, where $v_{\rm F}$ and $N(0)$ are the Fermi velocity

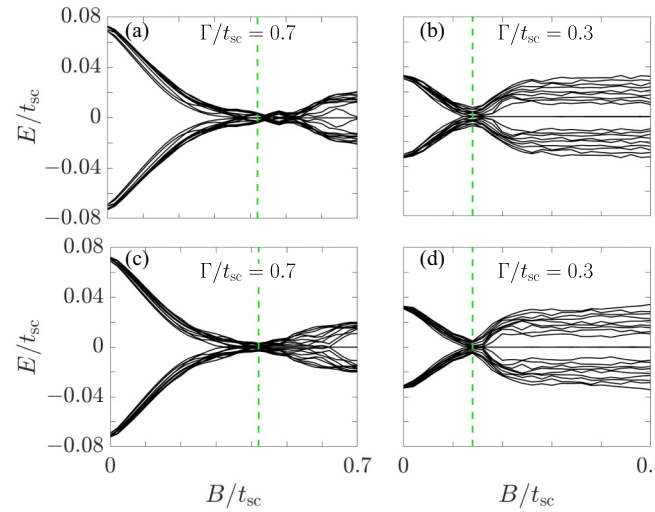

FIG. 5. Low-energy spectrum as a function of Zeeman field $B/t_{\rm sc}$ for a single realization of disorder present in all the components: SC, SM, and the interface. Top and bottom rows correspond to different disorder realizations. The left (right) column corresponds to strong (weak) coupling. Dashed green lines mark the topological phase transition point in the clean limit. All parameters are the same as Fig. 2 in the main text with disorder strengths $w_{\rm sc}/\mu_{\rm sc} = 1$, $w_{\rm SM}/\mu_{\rm SM} = 2$, and $w_\Gamma/\Gamma = 0.5$.

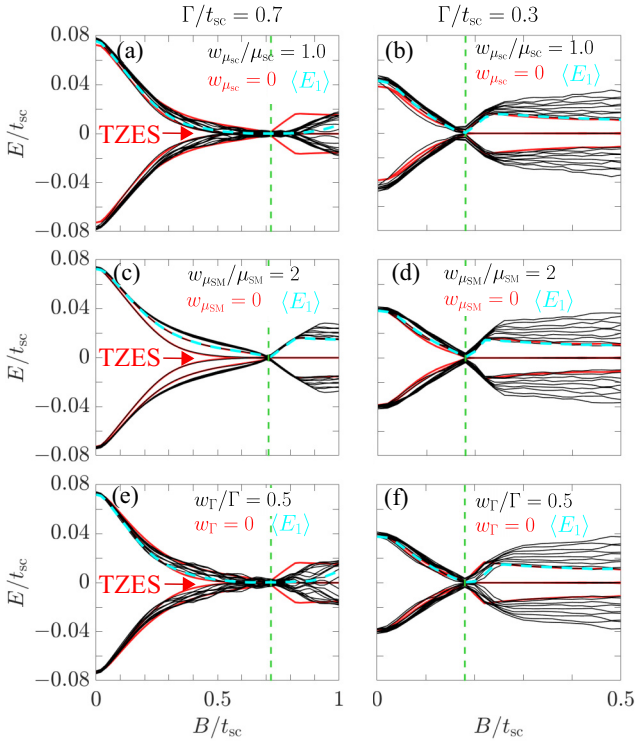

FIG. 6. Low-energy spectrum as a function of the Zeeman field B for a single disorder configuration (20 lowest levels, black), for disorder in (a) and (b) the SC and (c) and (d) SM and (e) and (f) at the interface for strong (left) and weak (right) coupling Γ. Clean system spectrum (only the four lowest levels, red) and disorder-averaged E_1 (30 configurations; cyan). Dashed green lines denote the TPT. Compare with Fig. 2 in the main text.

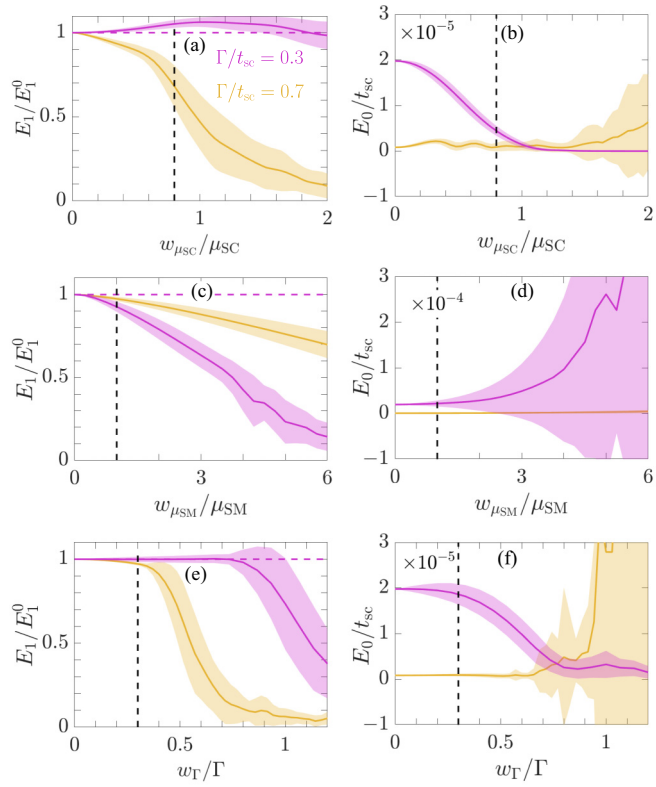

FIG. 7. Disorder-averaged calculations (30 random configurations) in the topological phase at $B/B_c = 1.5$ showing E_0/t_{SC} (left) and E_1/E_1^0 (right) as a function of disorder strength for disorder in (a) and (b) the SC and (c) and (d) SM and (e) and (f) at the interface for weak (purple) and strong (yellow) coupling Γ. Shaded regions represent one standard deviation. Compare with Fig. 4 in the main text. Vertical black dashed lines indicate the boundary between weak (left) and strong (right) disorder.

and normal state density of states, respectively, and are given by separate values in the SC and SM [52,58]. Also the superconducting coherence length is given by $\xi = v_F/\Delta$, where Δ is the superconducting order parameter, or, equivalently, gap, in the SC, while it is the proximity-induced (superconducting) gap Δ_{ind} in the SM.

To estimate the disorder strength required to be in the strong-disorder regime, we treat the SC and SM separately. We consider the parameters listed in the Sec. II. For the SC, we use the density of states for a 2D SC, which is $N(0) = m^*/(\pi\hbar^2) = 1/(2\pi t)$. We then obtain $\xi/l = w_{\mu_{SC}}^2/(2\Delta t)$, which for our parameters gives $\xi/l \gtrsim 1$ when $w_{\mu_{SC}} \gtrsim 0.4t_{SC}$. This results in the SC being in the strong-disorder regime for $w_{\mu_{SC}}/\mu_{SC} \gtrsim 0.8$, as stated in the main text. Similarly, for the 1D SM, we have $N(0) = 2/(\pi\hbar v_F)$. Thus, $\xi/l = 2w_{\mu_{SM}}^2/(\Delta_{ind} v_F)$ for the SM. For our parameter choices we find $\Delta_{ind} \approx 0.04t_{SC}$ ($\Delta_{ind} \approx 0.07t_{SC}$) for $\Gamma = 0.3t_{SC}$ ($\Gamma = 0.7t_{SC}$). We then find that the disorder strength for the strong-disorder regime must satisfy $w_{\mu_{SM}} \gtrsim 0.02t_{SM}$ ($w_{\mu_{SM}} \gtrsim 0.03t_{SM}$) for $\Gamma = 0.3t_{SC}$ ($\Gamma = 0.7t_{SC}$). This implies that $w_{\mu_{SM}}/\mu_{SM} \gtrsim 1$ characterizes the strong-disorder regime, as stated in the main text.

In the case of disorder at the interface, modeled as disorder in the coupling Γ, we follow a previous study [101] and consider fluctuations larger than 30% of the coupling strength to be in the strong-disorder regime. Thus, strong disorder here occurs for $w_\Gamma/\Gamma \gtrsim 0.3$, as stated in the main text.

APPENDIX B: DISORDER IN ALL COMPONENTS

In the main text we consider disorder in only one component of the SC-SM system at a time in order to identify which part is more or less detrimental and how it can be mitigated in the weak-coupling regime. In real samples, however, disorder is likely present in all parts of the system at the same time. In this Appendix we consider this situation and perform calculations for scalar disorder in all components simultaneously, i.e., in the SC and SM and at the interface. We plot the low-energy spectrum as a function of the Zeeman field in Fig. 5 for a single disorder realization at strong (left column) and weak coupling (right column). We observe that, for strong couplings, there is an avalanche of disorder-induced zero-energy states in both the trivial and topological regimes, which ruins the topological gap, any possible identification of the topological phase transition, and even clear detection of MBSs. In contrast, all these issues of the strong-coupling regime are mitigated at weak coupling: the formation of trivial zero-energy states is clearly suppressed, allowing us to identify a clear topological phase transition, while the absence

of in-gap states in the topological phase generates a robust topological gap and MBSs only at zero energy. Thus, even when disorder is present in all components of the SC-SM system, the weak-coupling regime proves to be beneficial for mitigating the formation of TZESs and detection of MBSs, thus supporting our findings in the main text.

APPENDIX C: INFLUENCE OF DISORDER ON A TZES APPEARING IN THE CLEAN LIMIT

In the main text we consider only systems that do not host any TZES in the clean limit, so that the TZES in the main text are all induced by disorder. For different parameter choices it is, however, possible to also have TZESs appearing in the N region of the SM in the clean regime, which we here simply refer to as clean-limit TZESs. These clean-limit TZESs occur due to the renormalization of the effective chemical potential in the SM, which, due to the uncovered N region in our case, acquires an inhomogeneous profile (see Refs. [45–47]). In this Appendix we provide additional data showing that our conclusions in the main text is not dependent on whether the clean limit hosts TZESs already or not. To achieve TZESs in the clean limit we change the parameters slightly from the main text by setting $\mu_{SC} = 0.5t_{SC}$ but keep all other parameters the same. This produces clean-limit TZESs in the N region in the strong-coupling regime.

In Fig. 6 we plot the low-energy spectrum as a function of the Zeeman field B for both the strong (left) and weak (right) coupling regimes for strong disorder in the SC (top), in the SM (middle), and at the interface (bottom). We compare these single-disorder results (black) with results for the clean system (red) and also the disorder-averaged E_1 (cyan). Thus, Fig. 6 is the same as Fig. 2 in the main text, except that in Fig. 6 we also have a TZES in the clean limit for strong coupling. Comparing Figs. 2 and 6 it is clear that the influence of disorder is very similar; namely, for disorder in the SC or at the interface, we find that at weak coupling there are no disorder-induced TZESs, while for strong coupling we clearly find additional disorder-induced TZESs close to the topological phase transition. For disorder in the SM, weak or strong coupling matters less, and the TZES in the clean limit for strong coupling is the only TZES in the system. These results are further solidified by studying the disorder-averaged E_1, which, for disorder both in the SC and at the interface, comes close to zero in the strong-coupling regime but is almost the same as in the clean system in the weak-coupling regime.

In Fig. 7 we plot disorder-averaged E_1 (left) and E_0 (right) in the topological phase for disorder in the SC (top), in the SM (middle), and at the interface (bottom) for both strong (yellow) and weak (purple) SC-SM coupling. Figure 7 is the equivalent of Fig. 4 in the main text, but now for a system with a TZES in the clean limit for strong coupling. By direct comparison we see that there are no qualitative changes in the results between Figs. 7 and 4. To summarize, the above results support the conclusions in the main text, in that the weak-coupling regime is more robust to disorder than the strong-coupling regime, irrespective of whether TZESs are present in clean limit with strong coupling or not.

[1] M. Leijnse and K. Flensberg, Introduction to topological superconductivity and Majorana fermions, Semicond. Sci. Technol. **27**, 124003 (2012).

[2] R. Aguado, Majorana quasiparticles in condensed matter, Riv. Nuovo Cimento **40**, 523 (2017).

[3] R. M. Lutchyn, E. P. A. M. Bakkers, L. P. Kouwenhoven, P. Krogstrup, C. M. Marcus, and Y. Oreg, Majorana zero modes in superconductor-semiconductor heterostructures, Nat. Rev. Mater. **3**, 52 (2018).

[4] H. Zhang, D. E. Liu, M. Wimmer, and L. P. Kouwenhoven, Next steps of quantum transport in Majorana nanowire devices, Nat. Commun. **10**, 5128 (2019).

[5] S. M. Frolov, M. J. Manfra, and J. D. Sau, Topological superconductivity in hybrid devices, Nat. Phys. **16**, 718 (2020).

[6] K. Laubscher and J. Klinovaja, Majorana bound states in semiconducting nanostructures, J. Appl. Phys. **130**, 081101 (2021).

[7] E. Prada, P. San-Jose, M. W. de Moor, A. Geresdi, E. J. Lee, J. Klinovaja, D. Loss, J. Nygård, R. Aguado, and L. P. Kouwenhoven, From Andreev to Majorana bound states in hybrid superconductor–semiconductor nanowires, Nat. Rev. Phys. **2**, 575 (2020).

[8] K. Flensberg, F. von Oppen, and A. Stern, Engineered platforms for topological superconductivity and Majorana zero modes, Nat. Rev. Mater. **6**, 944 (2021).

[9] P. Marra, Majorana nanowires for topological quantum computation, J. Appl. Phys. **132**, 231101 (2022).

[10] Y. Oreg, G. Refael, and F. von Oppen, Helical Liquids and Majorana Bound States in Quantum Wires, Phys. Rev. Lett. **105**, 177002 (2010).

[11] J. Alicea, Majorana fermions in a tunable semiconductor device, Phys. Rev. B **81**, 125318 (2010).

[12] R. M. Lutchyn, J. D. Sau, and S. Das Sarma, Majorana Fermions and a Topological Phase Transition in Semiconductor-Superconductor Heterostructures, Phys. Rev. Lett. **105**, 077001 (2010).

[13] Y. Tanaka and S. Kashiwaya, Theory of Tunneling Spectroscopy of d-Wave Superconductors, Phys. Rev. Lett. **74**, 3451 (1995).

[14] C. J. Bolech and E. Demler, Observing Majorana Bound States in p-Wave Superconductors Using Noise Measurements in Tunneling Experiments, Phys. Rev. Lett. **98**, 237002 (2007).

[15] K. T. Law, P. A. Lee, and T. K. Ng, Majorana Fermion Induced Resonant Andreev Reflection, Phys. Rev. Lett. **103**, 237001 (2009).

[16] K. Flensberg, Tunneling characteristics of a chain of Majorana bound states, Phys. Rev. B **82**, 180516(R) (2010).

[17] V. Mourik, K. Zuo, S. Frolov, S. Plissard, E. Bakkers, and L. Kouwenhoven, Signatures of Majorana fermions in hybrid superconductor-semiconductor nanowire devices, Science **336**, 1003 (2012).

[18] M. T. Deng, C. L. Yu, G. Y. Huang, M. Larsson, P. Caroff, and H. Q. Xu, Anomalous zero-bias conductance peak in a Nb–InSb nanowire–Nb hybrid device, Nano Lett. **12**, 6414 (2012).

[19] S. M. Albrecht, A. P. Higginbotham, M. Madsen, F. Kuemmeth, T. S. Jespersen, J. Nygård, P. Krogstrup, and C. M. Marcus, Exponential protection of zero modes in Majorana islands, Nature (London) **531**, 206 (2016).

[20] M. T. Deng, S. Vaitiekėnas, E. B. Hansen, J. Danon, M. Leijnse, K. Flensberg, J. Nygård, P. Krogstrup, and C. M. Marcus, Majorana bound state in a coupled quantum-dot hybrid-nanowire system, Science **354**, 1557 (2016).

[21] H. J. Suominen, M. Kjaergaard, A. R. Hamilton, J. Shabani, C. J. Palmstrøm, C. M. Marcus, and F. Nichele, Zero-Energy Modes from Coalescing Andreev States in a Two-Dimensional Semiconductor-Superconductor Hybrid Platform, Phys. Rev. Lett. **119**, 176805 (2017).

[22] F. Nichele, A. C. C. Drachmann, A. M. Whiticar, E. C. T. O'Farrell, H. J. Suominen, A. Fornieri, T. Wang, G. C. Gardner, C. Thomas, A. T. Hatke, P. Krogstrup, M. J. Manfra, K. Flensberg, and C. M. Marcus, Scaling of Majorana Zero-Bias Conductance Peaks, Phys. Rev. Lett. **119**, 136803 (2017).

[23] S. Vaitiekėnas, Y. Liu, P. Krogstrup, and C. Marcus, Zero-bias peaks at zero magnetic field in ferromagnetic hybrid nanowires, Nat. Phys. **17**, 43 (2021).

[24] T. Dvir, G. Wang, N. van Loo, C.-X. Liu, G. P. Mazur, A. Bordin, S. L. D. ten Haaf, J.-Y. Wang, D. van Driel, F. Zatelli, X. Li, F. K. Malinowski, S. Gazibegovic, G. Badawy, E. P. A. M. Bakkers, M. Wimmer, and L. P. Kouwenhoven, Realization of a minimal Kitaev chain in coupled quantum dots, Nature **614**, 445 (2023).

[25] E. Prada, P. San-Jose, and R. Aguado, Transport spectroscopy of NS nanowire junctions with Majorana fermions, Phys. Rev. B **86**, 180503(R) (2012).

[26] J. Liu, A. C. Potter, K. T. Law, and P. A. Lee, Zero-Bias Peaks in the Tunneling Conductance of Spin-Orbit-Coupled Superconducting Wires with and without Majorana End-States, Phys. Rev. Lett. **109**, 267002 (2012).

[27] C.-X. Liu, J. D. Sau, T. D. Stanescu, and S. Das Sarma, Andreev bound states versus Majorana bound states in quantum dot-nanowire-superconductor hybrid structures: Trivial versus topological zero-bias conductance peaks, Phys. Rev. B **96**, 075161 (2017).

[28] C. Moore, C. Zeng, T. D. Stanescu, and S. Tewari, Quantized zero-bias conductance plateau in semiconductor-superconductor heterostructures without topological Majorana zero modes, Phys. Rev. B **98**, 155314 (2018).

[29] J. Chen, B. D. Woods, P. Yu, M. Hocevar, D. Car, S. R. Plissard, E. P. A. M. Bakkers, T. D. Stanescu, and S. M. Frolov, Ubiquitous Non-Majorana Zero-Bias Conductance Peaks in Nanowire Devices, Phys. Rev. Lett. **123**, 107703 (2019).

[30] T. Dvir, M. Aprili, C. H. L. Quay, and H. Steinberg, Zeeman Tunability of Andreev Bound States in van der Waals Tunnel Barriers, Phys. Rev. Lett. **123**, 217003 (2019).

[31] A. Vuik, B. Nijholt, A. R. Akhmerov, and M. Wimmer, Reproducing topological properties with quasi-Majorana states, SciPost Phys. **7**, 061 (2019).

[32] Y. Zhang, K. Guo, and J. Liu, Transport characterization of topological superconductivity in a planar Josephson junction, Phys. Rev. B **102**, 245403 (2020).

[33] M. Valentini, F. Peñaranda, A. Hofmann, M. Brauns, R. Hauschild, P. Krogstrup, P. San-Jose, E. Prada, R. Aguado, and G. Katsaros, Nontopological zero-bias peaks in full-shell nanowires induced by flux-tunable Andreev states, Science **373**, 82 (2021).

[34] C. Jünger, R. Delagrange, D. Chevallier, S. Lehmann, K. A. Dick, C. Thelander, J. Klinovaja, D. Loss, A. Baumgartner, and C. Schönenberger, Magnetic-Field-Independent Subgap States in Hybrid Rashba Nanowires, Phys. Rev. Lett. **125**, 017701 (2020).

[35] D. Razmadze, E. C. T. O'Farrell, P. Krogstrup, and C. M. Marcus, Quantum Dot Parity Effects in Trivial and Topological Josephson Junctions, Phys. Rev. Lett. **125**, 116803 (2020).

[36] J. Cayao and P. Burset, Confinement-induced zero-bias peaks in conventional superconductor hybrids, Phys. Rev. B **104**, 134507 (2021).

[37] P. Yu, J. Chen, M. Gomanko, G. Badawy, E. P. A. M. Bakkers, K. Zuo, V. Mourik, and S. M. Frolov, Non-Majorana states yield nearly quantized conductance in superconductor-semiconductor nanowire devices, Nat. Phys. **17**, 482 (2021).

[38] P. Marra and A. Nigro, Majorana/Andreev crossover and the fate of the topological phase transition in inhomogeneous nanowires, J. Phys.: Condens. Matter **34**, 124001 (2022).

[39] R. Hess, H. F. Legg, D. Loss, and J. Klinovaja, Trivial Andreev Band Mimicking Topological Bulk Gap Reopening in the Nonlocal Conductance of Long Rashba Nanowires, Phys. Rev. Lett. **130**, 207001 (2023).

[40] X.-F. Chen, W. Luo, T.-F. Fang, Y. Paltiel, O. Millo, A.-M. Guo, and Q.-F. Sun, Topologically nontrivial and trivial zero modes in chiral molecules, arXiv:2208.13352.

[41] D. Sahu, V. Khade, and S. Gangadharaiah, Effect of topological length on bound states signatures in a topological nanowire, arXiv:2211.03045.

[42] G. Kells, D. Meidan, and P. W. Brouwer, Near-zero-energy end states in topologically trivial spin-orbit coupled superconducting nanowires with a smooth confinement, Phys. Rev. B **86**, 100503(R) (2012).

[43] J. Cayao, E. Prada, P. San-Jose, and R. Aguado, SNS junctions in nanowires with spin-orbit coupling: Role of confinement and helicity on the subgap spectrum, Phys. Rev. B **91**, 024514 (2015).

[44] M. W. A. de Moor, J. D. S. Bommer, D. Xu, G. W. Winkler, A. E. Antipov, A. Bargerbos, G. Wang, N. van Loo, R. L. M. O. het Veld, S. Gazibegovic, D. Car, J. A. Logan, M. Pendharkar, J. S. Lee, E. P. A. M. Bakkers, C. J. Palmstrøm, R. M. Lutchyn, L. P. Kouwenhoven, and H. Zhang, Electric field tunable superconductor-semiconductor coupling in Majorana nanowires, New J. Phys. **20**, 103049 (2018).

[45] O. A. Awoga, J. Cayao, and A. M. Black-Schaffer, Supercurrent Detection of Topologically Trivial Zero-Energy States in Nanowire Junctions, Phys. Rev. Lett. **123**, 117001 (2019).

[46] C. Reeg, O. Dmytruk, D. Chevallier, D. Loss, and J. Klinovaja, Zero-energy Andreev bound states from quantum dots in proximitized Rashba nanowires, Phys. Rev. B **98**, 245407 (2018).

[47] O. A. Awoga, J. Cayao, and A. M. Black-Schaffer, Robust topological superconductivity in weakly coupled nanowire-superconductor hybrid structures, Phys. Rev. B **105**, 144509 (2022).

[48] S. D. Escribano, A. Maiani, M. Leijnse, K. Flensberg, Y. Oreg, A. L. Yeyati, E. Prada, and R. S. Souto, Semiconductor-ferromagnet-superconductor planar heterostructures for 1D topological superconductivity, npj Quantum Mater. **7**, 81 (2022).

[49] O. Motrunich, K. Damle, and D. A. Huse, Griffiths effects and quantum critical points in dirty superconductors without spin-rotation invariance: One-dimensional examples, Phys. Rev. B **63**, 224204 (2001).

[50] P. W. Brouwer, M. Duckheim, A. Romito, and F. von Oppen, Topological superconducting phases in disordered quantum wires with strong spin-orbit coupling, Phys. Rev. B **84**, 144526 (2011).

[51] A. R. Akhmerov, J. P. Dahlhaus, F. Hassler, M. Wimmer, and C. W. J. Beenakker, Quantized Conductance at the Majorana Phase Transition in a Disordered Superconducting Wire, Phys. Rev. Lett. **106**, 057001 (2011).

[52] A. C. Potter and P. A. Lee, Engineering a $p+ip$ superconductor: Comparison of topological insulator and Rashba spin-orbit-coupled materials, Phys. Rev. B **83**, 184520 (2011).

[53] D. Bagrets and A. Altland, Class *D* Spectral Peak in Majorana Quantum Wires, Phys. Rev. Lett. **109**, 227005 (2012).

[54] R. M. Lutchyn, T. D. Stanescu, and S. Das Sarma, Momentum relaxation in a semiconductor proximity-coupled to a disordered *s*-wave superconductor: Effect of scattering on topological superconductivity, Phys. Rev. B **85**, 140513(R) (2012).

[55] F. Pientka, G. Kells, A. Romito, P. W. Brouwer, and F. von Oppen, Enhanced Zero-Bias Majorana Peak in the Differential Tunneling Conductance of Disordered Multisubband Quantum-Wire/Superconductor Junctions, Phys. Rev. Lett. **109**, 227006 (2012).

[56] D. I. Pikulin, J. P. Dahlhaus, M. Wimmer, H. Schomerus, and C. W. J. Beenakker, A zero-voltage conductance peak from weak antilocalization in a Majorana nanowire, New J. Phys. **14**, 125011 (2012).

[57] J. D. Sau and S. Das Sarma, Density of states of disordered topological superconductor-semiconductor hybrid nanowires, Phys. Rev. B **88**, 064506 (2013).

[58] W. S. Cole, J. D. Sau, and S. Das Sarma, Proximity effect and Majorana bound states in clean semiconductor nanowires coupled to disordered superconductors, Phys. Rev. B **94**, 140505(R) (2016).

[59] H. Pan and S. Das Sarma, Physical mechanisms for zero-bias conductance peaks in Majorana nanowires, Phys. Rev. Res. **2**, 013377 (2020).

[60] M. Thamm and B. Rosenow, Machine Learning Optimization of Majorana Hybrid Nanowires, Phys. Rev. Lett. **130**, 116202 (2023).

[61] H. Zhang *et al.*, Large zero-bias peaks in InSb-Al hybrid semiconductor-superconductor nanowire devices, arXiv:2101.11456.

[62] S. Ahn, H. Pan, B. Woods, T. D. Stanescu, and S. Das Sarma, Estimating disorder and its adverse effects in semiconductor Majorana nanowires, Phys. Rev. Mater. **5**, 124602 (2021).

[63] S. Das Sarma and H. Pan, Disorder-induced zero-bias peaks in Majorana nanowires, Phys. Rev. B **103**, 195158 (2021).

[64] D. Kuzmanovski, A. M. Black-Schaffer, and J. Cayao, Suppression of odd-frequency pairing by phase disorder in a nanowire coupled to Majorana zero modes, Phys. Rev. B **101**, 094506 (2020).

[65] M. Aghaee *et al.*, InAs-Al hybrid devices passing the topological gap protocol, arXiv:2207.02472.

[66] S. D. Sarma, In search of Majorana, Nat. Phys. **19**, 165 (2023).

[67] W. Chang, S. M. Albrecht, T. S. Jespersen, F. Kuemmeth, P. Krogstrup, J. Nygård, and C. M. Marcus, Hard gap in epitaxial semiconductor–superconductor nanowires, Nat. Nanotechnol. **10**, 232 (2015).

[68] E. J. H. Lee, X. Jiang, R. Žitko, R. Aguado, C. M. Lieber, and S. De Franceschi, Scaling of subgap excitations in a superconductor-semiconductor nanowire quantum dot, Phys. Rev. B **95**, 180502(R) (2017).

[69] C. Reeg, D. Loss, and J. Klinovaja, Metallization of a Rashba wire by a superconducting layer in the strong-proximity regime, Phys. Rev. B **97**, 165425 (2018).

[70] C. Reeg, D. Loss, and J. Klinovaja, Finite-size effects in a nanowire strongly coupled to a thin superconducting shell, Phys. Rev. B **96**, 125426 (2017).

[71] T. D. Stanescu and S. Das Sarma, Proximity-induced low-energy renormalization in hybrid semiconductor-superconductor Majorana structures, Phys. Rev. B **96**, 014510 (2017).

[72] P. W. Anderson, Absence of diffusion in certain random lattices, Phys. Rev. **109**, 1492 (1958).

[73] T. Löthman, C. Triola, J. Cayao, and A. M. Black-Schaffer, Disorder-robust *p*-wave pairing with odd-frequency dependence in normal metal–conventional superconductor junctions, Phys. Rev. B **104**, 094503 (2021).

[74] M. Mashkoori, F. Parhizgar, S. Rachel, and A. M. Black-Schaffer, Detrimental effects of disorder in two-dimensional time-reversal invariant topological superconductors, Phys. Rev. B **107**, 014512 (2023).

[75] For a N region with a vanishing length, $L_{\mathrm{N}}=0$, we have verified that our results do not change.

[76] W. E. Arnoldi, The principle of minimized iterations in the solution of the matrix eigenvalue problem, Q. Appl. Math. **9**, 17 (1951).

[77] A. Maiani, R. Seoane Souto, M. Leijnse, and K. Flensberg, Topological superconductivity in semiconductor-superconductor-magnetic-insulator heterostructures, Phys. Rev. B **103**, 104508 (2021).

[78] The vanishing of the gap depends on system size: short SMs develop a sharp profile at the TPT, but E_0 does not usually reach zero, while for long systems E_0 reaches zero.

[79] S. D. Sarma, M. Freedman, and C. Nayak, Majorana zero modes and topological quantum computation, npj Quantum Inf. **1**, 15001 (2015).

[80] We have checked that other random disorder realizations support our claims.

[81] To be precise, in the strong-coupling regime, while most of the wave functions of the TZESs are mostly located in the SC, some of them are also in the SM, but that portion is much smaller.

[82] P. Anderson, Theory of dirty superconductors, J. Phys. Chem. Solids **11**, 26 (1959).

[83] L. P. Gor'kov and E. I. Rashba, Superconducting 2D System with Lifted Spin Degeneracy: Mixed Singlet-Triplet State, Phys. Rev. Lett. **87**, 037004 (2001).

[84] F. S. Bergeret, A. F. Volkov, and K. B. Efetov, Odd triplet superconductivity and related phenomena in superconductor-ferromagnet structures, Rev. Mod. Phys. **77**, 1321 (2005).

[85] J. Linder and J. W. Robinson, Superconducting spintronics, Nat. Phys. **11**, 307 (2015).

[86] X. Liu, J. D. Sau, and S. Das Sarma, Universal spin-triplet superconducting correlations of Majorana fermions, Phys. Rev. B **92**, 014513 (2015).

[87] S. H. Jacobsen, J. A. Ouassou, and J. Linder, Superconducting order in magnetic heterostructures, in *Advanced Magnetic and Optical Materials* (Wiley, Hoboken, NJ, 2016), Chap. 1, pp. 1–46.

[88] J. Cayao and A. M. Black-Schaffer, Odd-frequency superconducting pairing in junctions with Rashba spin-orbit coupling, Phys. Rev. B **98**, 075425 (2018).

[89] S. Tamura, S. Hoshino, and Y. Tanaka, Odd-frequency pairs in chiral symmetric systems: Spectral bulk-boundary correspondence and topological criticality, Phys. Rev. B **99**, 184512 (2019).

[90] A. Tsintzis, A. M. Black-Schaffer, and J. Cayao, Odd-frequency superconducting pairing in Kitaev-based junctions, Phys. Rev. B **100**, 115433 (2019).

[91] J. Cayao, C. Triola, and A. M. Black-Schaffer, Odd-frequency superconducting pairing in one-dimensional systems, Eur. Phys. J.: Spec. Top. **229**, 545 (2020).

[92] In addition to the chemical potential, other parameters such as spin-orbit coupling and the g factor also suffer renormalization in the strong-coupling regime.

[93] O. A. Awoga, K. Björnson, and A. M. Black-Schaffer, Disorder robustness and protection of Majorana bound states in ferromagnetic chains on conventional superconductors, Phys. Rev. B **95**, 184511 (2017).

[94] A. Haim and A. Stern, Benefits of Weak Disorder in One-Dimensional Topological Superconductors, Phys. Rev. Lett. **122**, 126801 (2019).

[95] F. Domínguez, J. Cayao, P. San-Jose, R. Aguado, A. L. Yeyati, and E. Prada, Zero-energy pinning from interactions in Majorana nanowires, npj Quantum Mater. **2**, 13 (2017).

[96] B. D. Woods, T. D. Stanescu, and S. Das Sarma, Effective theory approach to the Schrödinger-Poisson problem in semiconductor Majorana devices, Phys. Rev. B **98**, 035428 (2018).

[97] S. D. Escribano, A. L. Yeyati, and E. Prada, Interaction-induced zero-energy pinning and quantum dot formation in Majorana nanowires, Beilstein J. Nanotechnol. **9**, 2171 (2018).

[98] A. E. G. Mikkelsen, P. Kotetes, P. Krogstrup, and K. Flensberg, Hybridization at Superconductor-Semiconductor Interfaces, Phys. Rev. X **8**, 031040 (2018).

[99] A. E. Antipov, A. Bargerbos, G. W. Winkler, B. Bauer, E. Rossi, and R. M. Lutchyn, Effects of Gate-Induced Electric Fields on Semiconductor Majorana Nanowires, Phys. Rev. X **8**, 031041 (2018).

[100] R. M. Lutchyn, T. D. Stanescu, and S. Das Sarma, Search for Majorana Fermions in Multiband Semiconducting Nanowires, Phys. Rev. Lett. **106**, 127001 (2011).

[101] T. D. Stanescu, R. M. Lutchyn, and S. Das Sarma, Majorana fermions in semiconductor nanowires, Phys. Rev. B **84**, 144522 (2011).

[102] P. San-Jose, E. Prada, and R. Aguado, Mapping the Topological Phase Diagram of Multiband Semiconductors with Supercurrents, Phys. Rev. Lett. **112**, 137001 (2014).

[103] J. S. Lim, L. Serra, R. López, and R. Aguado, Magnetic-field instability of Majorana modes in multiband semiconductor wires, Phys. Rev. B **86**, 121103(R) (2012).

[104] A. C. Potter and P. A. Lee, Multichannel Generalization of Kitaev's Majorana End States and a Practical Route to Realize Them in Thin Films, Phys. Rev. Lett. **105**, 227003 (2010).

[105] S. Datta, *Electronic Transport in Mesoscopic Systems* (Cambridge University Press, Cambridge, 1997).